Journal of Catalysis 257 (2008) 96–107

Contents lists available at ScienceDirect

Journal of Catalysis

www.elsevier.com/locate/jcat

Hydrogen production from ethanol over Ir/CeO_2 catalysts: A comparative study of steam reforming, partial oxidation and oxidative steam reforming

Weijie Cai [a], Fagen Wang [a], Ensheng Zhan [a], A.C. Van Veen [b], Claude Mirodatos [b], Wenjie Shen [a,*]

[a] State Key Laboratory of Catalysis, Dalian Institute of Chemical Physics, Chinese Academy of Sciences, Dalian 116023, China
[b] University of Lyon; Institut de Recherches sur la Catalyse et l'Environnement de Lyon (IRCELYON, UMR 5256, CNRS; Université Claude Bernard Lyon 1), 69626 Villeurbanne Cedex, France

ARTICLE INFO

Article history:
Received 2 February 2008
Revised 15 April 2008
Accepted 16 April 2008
Available online 21 May 2008

Keywords:
Ethanol
Hydrogen
Ir/CeO_2
Reaction pathway
Stability

ABSTRACT

Steam reforming, partial oxidation, and oxidative steam reforming of ethanol over Ir/CeO_2 catalysts were studied to elucidate the reaction pathway and determine catalytic stability. Temperature-programmed desorption and surface reaction revealed that ethoxy species were immediately formed on ethanol adsorption at room temperature, and were mainly further oxidized to acetate and carbonate species that finally decomposed into CH_4/CO and CO_2, respectively. Under reaction conditions, acetaldehyde was the primary product below 673 K, which decomposed mainly to methane and carbon monoxide at higher temperatures, whereas methane reforming and the water–gas shift were the major reactions above 773 K. The Ir/CeO_2 catalyst demonstrated rather high stability for the reactions at 823 and 923 K with no apparent deactivation for 60 h on stream; the mean size of Ir particles was stable at around 2–3 nm, but the ceria particles sintered significantly from 6–8 to 14–27 nm. CeO_2 likely prevented the highly dispersed Ir particles from sintering and inhibited coke deposition through strong Ir–CeO_2 interactions.

1. Introduction

Bioethanol, a mixture of water and ethanol produced by fermentation of biomass, is considered as an attractive feedstock for the sustainable production of hydrogen for fueling polymer electrolyte fuel cells [1–3]. Steam reforming (SR), partial oxidation (POX), and oxidative steam reforming (OSR) are effective routes for producing hydrogen from bioethanol. Most studies have focused on the SR of ethanol using supported Ni, Co, and Rh catalysts operated at relatively high temperatures, typically 873–1073 K [4–14]. Among these catalysts, Rh is the most effective system with respect to ethanol conversion and hydrogen selectivity [4–7], probably due to its strong capacity for breaking the C–C bond of ethanol,

$$CH_3CH_2OH + 3H_2O \rightarrow 6H_2 + 2CO_2. \quad (1)$$

But this reaction is highly endothermic, requiring large amounts of energy, which is a serious drawback to the cost and practicality of hydrogen production, especially for on-board applications.

POX of ethanol is an alternative route for the production of hydrogen using supported Ni, Ru, Pt, and Rh catalysts [15–17]. Ni catalysts exhibited adequate activity for ethanol conversion, but resulted in lower hydrogen productivity [17]. Again, Rh/CeO_2 catalysts were significantly more active and selective at 873–1273 K [15],

$$CH_3CH_2OH + 1.5O_2 \rightarrow 3H_2 + 2CO_2. \quad (2)$$

POX is exothermic and fast, making it suitable for coping with rapid load variations, such as those required for on-board reformers, which often work under non-steady-state conditions. However, the yield of hydrogen is much lower than that from SR.

OSR of ethanol, being a combination of SR and POX, constitutes a reasonable compromise between energy efficiency and hydrogen productivity. With a suitable mixture of ethanol, water, and oxygen, the exothermic POX of ethanol provides the heat necessary for the endothermic SR of ethanol. Moreover, the presence of oxygen in the reaction mixture also promotes the efficient removal of carbon species formed during the course of reaction. Using ethanol, water, and oxygen at a molar ratio of 1:1.8:0.6, the overall reaction can be thermally neutral ($\Delta H^{o}_{298} = +4.4$ kJ mol^{-1}), and the concentration of hydrogen can approach ~70% in the outlet stream [18]. Supported Ni, Pt, Rh, and Ir catalysts were reported to be effective for this reaction [18–26],

$$CH_3CH_2OH + 1.8H_2O + 0.6O_2 \rightarrow 4.8H_2 + 2CO_2. \quad (3)$$

The reaction mechanism has been extensively examined for the foregoing reactions, and adequate properties in terms of activity and hydrogen productivity have been achieved. But the catalytic stability, which is adversely affected by coke formation during the course of reaction, is rarely addressed and remains an open issue

* Corresponding author. Fax: +86 411 84694447.
E-mail address: shen98@dicp.ac.cn (W. Shen).

0021-9517/$ – see front matter
doi:10.1016/j.jcat.2008.04.009

for practical applications. We previously reported that Ir/CeO_2 catalysts showed excellent stability for SR and OSR of ethanol at relatively low temperatures using approximately stoichiometric feed streams [4,23].

In the present work, we extended our studies to the reaction pathway and catalytic stability for SR, POX, and OSR of ethanol over the Ir/CeO_2 catalyst. We first performed infrared spectroscopy of adsorbed ethanol and temperature-programmed surface reaction of ethanol studies to establish the key features of the reaction mechanism, and then compared the temperature-dependence of SR, POX and OSR of ethanol in terms of hydrogen yield and product distribution. Finally, we investigated the stability of the Ir/CeO_2 catalyst under stoichiometric reaction conditions in terms of structural changes derived from X-ray power diffraction (XRD) patterns and high-resolution transmission electron microscopy (HRTEM).

2. Experimental

2.1. Catalyst preparation

CeO_2 was prepared by precipitation of ammonia cerium nitrate with urea in an aqueous solution. First, 60 g of $(NH_4)_2Ce(NO_3)_6$ and 200 g of urea were dissolved into 2000 ml of water, and the mixture was heated gradually to 363 K under stirring and kept at this temperature for 27 h. After filtration and thorough washing with water, the precipitate was dried at 373 K for 12 h, then calcined for at 673 K for 5 h in air. The Ir/CeO_2 catalyst with an Ir nominal loading of 2 wt% was prepared by a deposition-precipitation method. CeO_2 powder was suspended in aqueous solution containing appropriate amounts of Ir precursor ($H_2IrCl_6{\cdot}6H_2O$), and the mixture was heated to 348 K under stirring. A 0.25 M Na_2CO_3 aqueous solution was added gradually until the pH value of the mixture reached 9.0, followed by further aging at 348 K for 1 h, during which the precipitate was exclusively deposited on the ceria surface. After filtration and washing with water, the solid obtained was dried at 373 K overnight and finally calcined at 673 K for 5 h in air.

2.2. Catalyst characterization

N_2 adsorption–desorption isotherms were recorded at 77 K using a Quantachrome Nova 4200e instrument. Before the measurements, the sample was degassed at 573 K for 2 h. The specific surface area was calculated by multipoint Braunauer–Emmett–Teller (BET) analysis of the nitrogen adsorption isotherms. The actual loading of Ir was analyzed by inductively coupled plasma atomic emission spectrometry (ICP-AES), using a PLASMA-SPEC-II device. An appropriate amount of sample was dissolved in aqua regia, and the resulting mixture was diluted with nitric acid to meet the detection range of the instrument.

XRD patterns were recorded using a Rigaku D/MAX-RB diffractor with Cu$K\alpha$ radiation source operating at 40 kV and 100 mA. Measurements of the reduction of the Ir/CeO_2 catalyst were performed in a high-temperature cell installed in the diffractometer. The sample was pressed into a pellet and mounted in the chamber. After heating to 473 K under a stream of He, the 5 vol% H_2/He mixture was introduced to the chamber for stepwise heating to the desired temperature (between 473 and 873 K) for 1 h before the XRD patterns were recorded. The mean crystallite size of ceria was calculated using Scherrer's equation [27].

HRTEM images were obtained using a Philips Tecnai $G^2$20 microscope operating at 300 kV. Specimens were prepared by ultrasonically suspending the sample in ethanol. A drop of the suspension was deposited to a thin carbon film supported on a standard copper grid and dried in air.

Oxygen storage capacity (OSC) was measured in a microreactor coupled to a quadrupole mass spectrometer (Omnistar, Balzers). Before analysis, the samples (100 mg) were reduced with 5% H_2/Ar (50 ml/min) at 923 K. The sample was purged for 15 min at 923 K using flowing Ar, and then cooled to 723 K. A 5% O_2/Ar mixture (50 ml/min) was then passed through the sample, and the oxygen consumption was measured with a mass spectrometer at $m/e = 32$.

Fourier transform infrared (FTIR) spectroscopy analysis of adsorbed ethanol was performed with a Brucker Vector 22 spectrometer in diffuse reflectance infrared Fourier transform (DRIFT) mode. Before the analysis, the sample was reduced with 5% H_2/He at 673 K for 1 h. After reduction, the system was purged with He at 673 K for 30 min and cooled to room temperature. The adsorption of ethanol was carried out at room temperature with a flowing mixture of ethanol/He for 1 h, which was obtained by passing He through a saturator containing ethanol at 273 K. After adsorption, the sample was purged with He for 30 min and then heated at a rate of 15 K/min up to 673 K. The spectra were recorded at room temperature and at 373, 473, 573, and 673 K.

2.3. Temperature-programmed desorption, surface reaction, and oxidation

Temperature-programmed desorption (TPD) and surface reaction (TPSR) of ethanol on the Ir/CeO_2 catalyst were conducted in a microreactor equipped with an online mass spectrometer (Omnistar, Balzers). Before testing, the catalyst (100 mg) was reduced with 5% H_2/He (40 ml/min) at 673 K for 1 h. After reduction, the system was purged with He at 673 K for 30 min and then cooled to room temperature. The adsorption of ethanol was carried out at room temperature with a flow of ethanol/He mixture for 1 h, obtained by passing He through a saturator containing ethanol at 273 K. After adsorption, the sample was purged with He (40 ml/min) for 30 min, and then heated at a rate of 15 K/min up to 973 K with flows of pure He (for TPD), 3.0% H_2O/He, 1.0% O_2/He, and 3.0% H_2O/1.0% O_2/He (for TPSR). The relative yields of C-containing products were calculated following the procedure described by Yee et al. [28].

Temperature-programmed oxidation (TPO) of the used catalyst was conducted in the same apparatus. Here 100 mg of the used catalyst was loaded, and the system was heated from 298 K to 973 K at a rate of 5 K/min with a flow of 5.0% O_2/Ar mixture (100 ml/min). The effluent was detected by mass spectrometry.

2.4. Catalytic measurements

Catalytic reactions were conducted in a continuous-flow fixed-bed quartz microreactor at atmospheric pressure. For this, 300 mg of catalyst (40–60 mesh) was loaded and sandwiched by two layers of quartz wool. Before the reaction, the catalyst was reduced with 5 vol% H_2/He (30 ml/min) at 673 K for 1 h. SR and OSR reactions were carried out with stoichiometric feed compositions of ethanol/water (1:3 molar ratio) and ethanol/water/O_2 (1:1.8:0.6 molar ratio), respectively. For comparison, POX was carried out using a feed composition of ethanol/O_2 (1:0.6 molar ratio). The gas hourly space velocity (GHSV) was 6000 ml/g_{cat}/h. Pure ethanol or aqueous ethanol solution were fed by a micropump to a vaporizer heated to 473 K, and the vapors were mixed with the oxygen stream coming from a mass-flow controller. The effluent from the reactor was analyzed by online gas chromatography. H_2, CO, and CO_2 were separated by a packed column (HayeSep D) and analyzed by a thermal conductivity detector (TCD) using He as carrier gas. Hydrocarbons and oxygenates were separated with a capillary column (INNOWAX) and analyzed with a flame ionization detector (FID).

3. Results and discussion

3.1. Structural properties of the Ir/CeO_2 catalyst

ICP analysis revealed that the amount of Ir in the Ir/CeO_2 catalyst was 2.1 wt%, as targeted. The loading of Ir decreased the specific surface area of ceria only slightly, from 158 to 153 m^2/g.

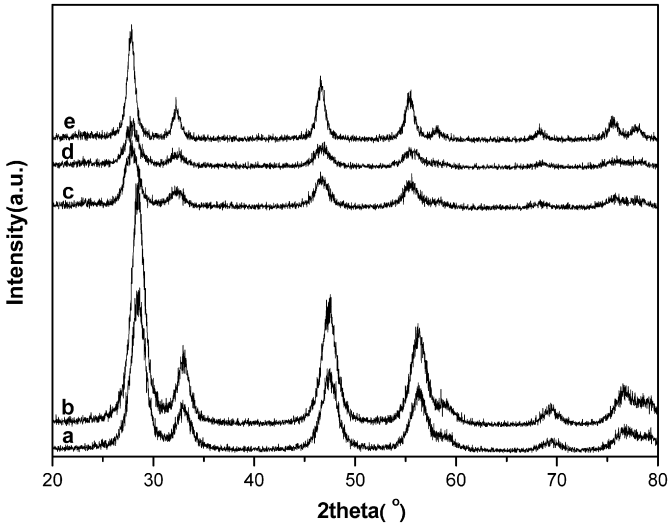

Fig. 1. XRD patterns of CeO_2 (a), the as-prepared Ir/CeO_2 catalyst (b) and the Ir/CeO_2 catalysts after reduction with hydrogen at 473 K (c), 673 K (d) and 873 K (e).

Fig. 1 shows the XRD patterns of the Ir/CeO_2 catalysts. Only the diffraction peaks of ceria with fluorite structure were observed for the as-prepared catalyst, and the average crystalline size was about 6 nm. This is in good agreement with the value (5.2 nm) estimated from the surface area. The absence of diffraction peaks from Ir species indicated that Ir crystalline was highly dispersed on CeO_2 and was too small to be detected. When the Ir/CeO_2 catalyst was reduced with hydrogen at 473 and 673 K, the crystallite sizes of ceria were still ~6 nm, suggesting that no sintering had occurred. But the position of diffraction peaks shifted to lower 2θ values, and the diffraction intensities became weaker. This was caused by defects formed through the reduction of surface CeO_2, because the radius of Ce^{3+} ions produced by ceria reduction was greater than that of Ce^{4+} ions (0.114 nm vs 0.097 nm) [29]. At 873 K, the diffraction peaks of CeO_2 in the reduced catalyst became sharper, and the crystallite size of ceria increased to 9.6 nm. In all cases, no diffraction peaks of Ir metal were detected, however, suggesting that the Ir particles were highly dispersed on ceria.

Fig. 2 shows the HRTEM images of the as-prepared Ir/CeO_2 catalyst. Ceria particle size ranged from 5 to 10 nm, in good accordance with XRD and BET measurements. Spherical ceria particles were poorly crystalline, and their composites were oriented randomly and interfaced epitaxially. Ir particles were difficult to see, likely due to their rather small size, but EDX analysis confirmed the presence of Ir on the CeO_2 surface.

OSC of the Ir/CeO_2 catalyst indicated a strong interaction between Ir and ceria. Oxygen uptake was 235 μmol O_2/g for the pure ceria and 596 μmol O_2/g for the Ir/CeO_2 catalyst. In fact, ceria is known to have an intrinsically high OSC, and the addition of noble metals could promote this property significantly [29–31]. This

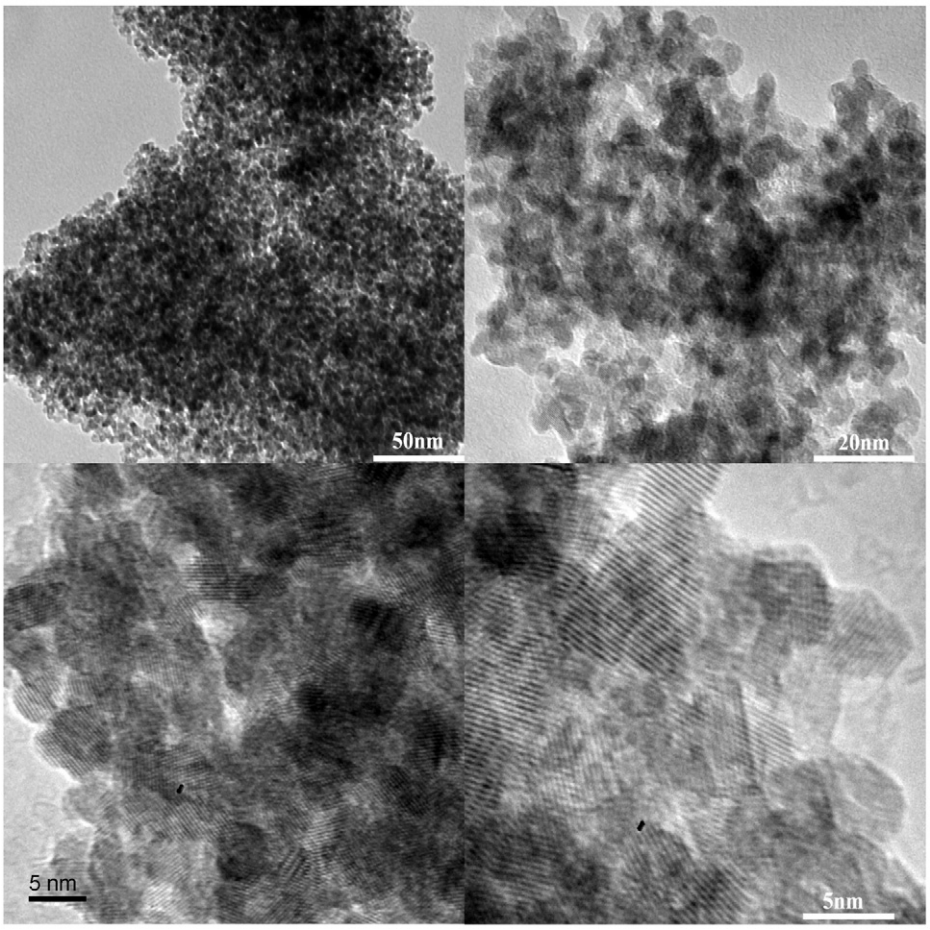

Fig. 2. HRTEM images of the as-prepared Ir/CeO_2 catalyst.

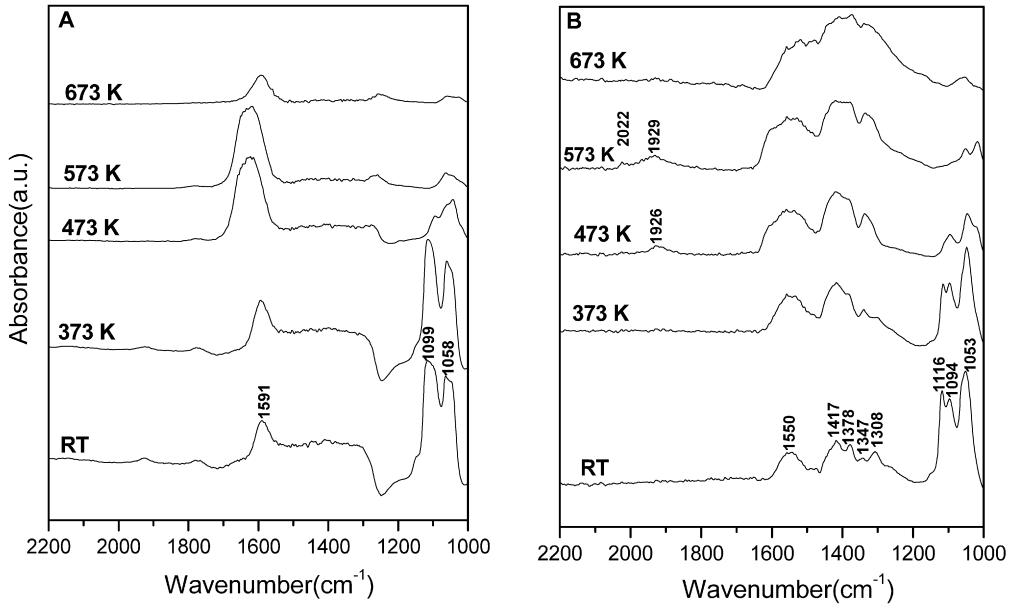

Fig. 3. FTIR spectra of ethanol adsorption on CeO_2 (A) and Ir/CeO_2 (B).

capacity is associated to the storage/release of oxygen through the Ce^{4+}/Ce^{3+} redox cycle. The specific role of the noble metal in OSC enhancement remains a matter of debate. One possible explanation is that part of the added metal forms small oxide clusters within the ceria fluorite structure, acting as privileged pathway for oxygen diffusion and storing [30,31]. Our previous temperature-programmed reduction (TPR) results with the Ir/CeO_2 catalyst indicated that the reduction of ceria was much easier after the addition of Ir, likely due to the strong Ir–ceria interaction [23]. We proposed that Ir effectively activated hydrogen molecules, which subsequently spilled over to the surface CeO_2 and reduced it at low temperatures. This observation is in good agreement with previous findings concerning the reduction of ceria-supported noble metal catalysts [29–31].

3.2. FTIR of ethanol activation

Fig. 3A shows the IR spectra of adsorbed ethanol on pure CeO_2. At room temperature, two types of ethoxy species were formed, characterized by (C–O) bands at 1099 and 1058 cm^{-1} as monodentate and bidentate species, respectively [32,34]. These two bands corresponded to a combination of νC–C and νC–O stretching vibrations, and to the νC–O stretching vibration of a bidentate system in which the O atom was shared between two adjacent cerium cations (Table 1). Indeed, adsorption of ethanol on ceria may occur readily through activation of the O–H bond to form an ethoxy species bonded to a surface cation of ceria [32–34].

Adsorbed acetate species were observed as a band at 1591 cm^{-1}. Most likely, the adsorbed ethoxy species underwent dehydrogenation to acetaldehyde, which further reacted with the surface –OH groups on ceria and produced acetate species [34,35]. Thus, both ethoxy and acetate species were readily formed on the CeO_2 surface on adsorption of ethanol at room temperature. This demonstrates that the dissociation of ethanol and the reaction of adsorbed ethoxy species were quite rapid and occurred simultaneously on the ceria surface. The intensity of the ethoxy species decreased progressively on heating, almost vanishing by 673 K. The intensity of the acetate species increased with increasing temperature up to 573 K and then decreased, indicating their decomposition. But no bands associated with carbonates appeared in the νC–O stretching range of 1000–1200 cm^{-1}, even at 673 K, confirming that ethoxy and acetate species were the only adsorbed intermediates formed on ceria after adsorption of ethanol.

Table 1
Bands (in cm^{-1}) of surface species produced by the adsorption of ethanol on CeO_2 and Ir/CeO_2

Vibrational mode	Ir/CeO_2	CeO_2
Ethoxy species		
νCO-monodentate	1116	1099
νCO-bidentate	1053	1058
$\delta_s CH_3$	1378	–
Acetate species		
δCH_3	1308	–
$\nu_s OCO$	1417	–
$\nu_{as} OCO$	1550	1591
Carbonate species		
ν_sOCO-monodentate	1347	–
CO		
νCO linear	2022	–
νCO bridging	1926	–

Fig. 3B shows the IR spectra of adsorbed ethanol on the Ir/CeO_2 catalyst. As mentioned above, the bands at 1094 and 1053 cm^{-1} are assigned to monodentate and bidentate ethoxy species, respectively, adsorbed on CeO_2 at room temperature. The bands at 1116 and 1378 cm^{-1} represent νCO and $\delta_s CH_3$ in ethoxy species [28], respectively. The bands at 1308, 1417, and 1550 cm^{-1} represent the acetate species formed through the surface reaction of ethoxy species. The new band at 1347 cm^{-1}, characteristic of monodentate carbonates (Table 1), indicates that further reaction of the acetate species produced carbonate species [34,35]. According to the assignments of vibrational modes for acetate and carbonate species, although it is difficult to identify a species simply by its vibrational modes in the C–O stretching region, evidence for the formation of carbonate species was obtained by heating the surface. As shown in Fig. 3B, the intensity of the bands attributed to ethoxy species decreased greatly on heating. At 473 K, the band at 1116 cm^{-1} almost disappeared, and the bands characteristic of linear carbonyl species adsorbed on Ir appeared at 1926 cm^{-1}, indicating the decomposition of ethoxy species on Ir particles [31,35]. When the temperature was increased to 573 K, the ethoxy species adsorbed on the ceria were decomposed to CO. As a result, car-

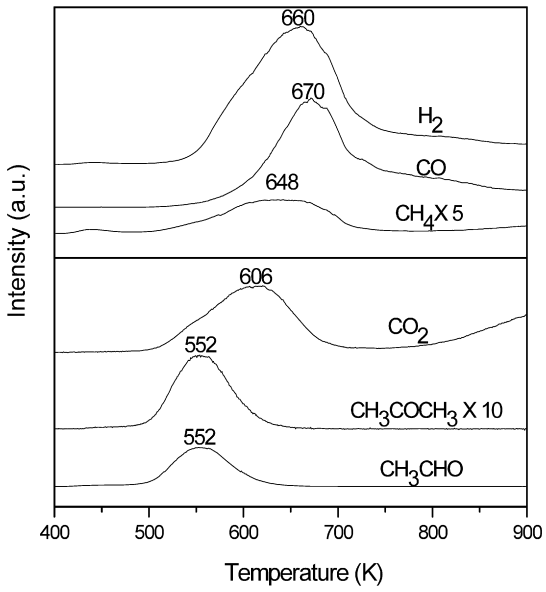

Fig. 4. TPD profile of ethanol adsorbed on the Ir/CeO_2 catalyst.

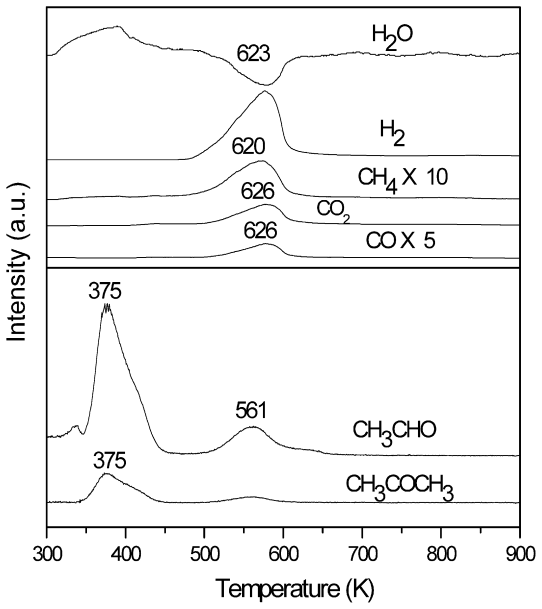

Fig. 5. Temperature-programmed surface reaction of adsorbed ethanol on the Ir/CeO_2 catalyst with a flow of 3.0% H_2O/He mixture.

bonyl bands at 1929 and 2022 cm^{-1} were clearly visible, and the ethoxy species disappeared almost completely at 673 K. In contrast, the intensity of the bands associated with acetate and carbonate species increased gradually, confirming the transformation of ethoxy species into acetate and carbonate species by interaction with ceria. At 673 K, all bands attributed to ethoxy species disappeared, and the bands representing acetate species also decreased significantly. The band characteristic of carbonate species at 1347 cm^{-1} became dominant, demonstrating that most of the acetate species were converted to carbonate species.

These findings clearly demonstrate that ethoxy species were formed immediately on the adsorption of ethanol on the Ir/CeO_2 catalyst, and that a fraction of these ethoxy species were further transformed into acetate and carbonate species even at room temperature. Increasing the temperature to 473–573 K led to the decomposition of ethoxy species into CO and methane, in addition to the formation of acetate and carbonate species. The formation of ethoxy and acetate species by ethanol adsorption at room temperature has been observed on CeO_2 [34], Pd/CeO_2 [31,34], and Rh/CeO_2 [36] catalysts, but the formation of carbonate species on ceria promoted by addition of a noble metal has not been reported.

3.3. TPD/TPSR of ethanol

3.3.1. TPD

Fig. 4 shows the TPD profile of ethanol adsorbed onto the pre-reduced Ir/CeO_2 catalyst. As revealed by the FTIR analysis, ethoxy, acetate, and carbonate species were readily formed on adsorption of ethanol at room temperature. Simultaneous desorption of acetaldehyde and acetone was observed at ~552 K. The former product is obviously due to the dehydrogenation of ethoxy species, and the latter likely comes from the further condensation of acetaldehyde, which is known to occur on basic surfaces like ceria. Desorption of CH_4 and CO_2 also began at ~552 K, presenting maxima at 606 and 648 K, respectively. Significant formation of H_2 and CO was observed at 660 and 670 K. This sequence is clearly related to the decomposition of the acetate and carbonate species initially formed from the ethoxy species.

The decomposition of carbonate species usually resulted in the formation of CO_2. However, the amount of CO_2 formed was very small compared with the amount expected based on the high coverage of carbonates initially formed on ceria. This may be because the CO_2 formed from carbonate decomposition reacted immediately with the oxygen vacancies of ceria to form new surface oxygen ions, releasing CO at ~670 K [31,37,38].

There have been several reports on ethanol desorption over Rh/CeO_2 and Pt/CeO_2 catalysts where the formation of CH_4, CO, and H_2 occurred at ~480 and above 500 K [31–33,39]. The low- and high-temperature desorption peaks were attributed to the decomposition of ethoxy species and acetate species, respectively. Here, only one intense peak of H_2, CO, and CH_4 was obtained in the temperature range of 640–670 K. It is highly possible that most of the ethoxy species were rapidly converted into acetate and carbonate species on the surface of ceria on heating, as demonstrated by the FTIR spectra. The decomposition of acetate species was responsible for the formation of CO and CH_4, whereas the formation of CO_2 at 606–670 K should be due mainly to the decomposition of carbonate species.

3.3.2. TPSR

Adding water and/or oxygen to the carrier gas significantly modified the TPD and TPSR desorption features. As shown in Fig. 5, adding water to the carrier gas shifted the formation of acetaldehyde and acetone to 375 K, much lower than that in the TPD experiment. This indicates that water enhanced the dehydrogenation of ethoxy species to acetaldehyde, favoring ready desorption of acetaldehyde and thus inhibiting the formation of acetate species. Significant water consumption occurred at ~623 K, and the formation of considerable amounts of H_2 and CO_2 occurred at ~626 K. Meanwhile, trace amounts of CH_4 and CO also were produced. This provides evidence that the decomposition of the acetate and carbonate species occurred mainly in this temperature region.

Fig. 6 shows the TPSR profile of ethanol with the O_2/He mixture. Desorption of acetaldehyde was observed at ~362 K. In parallel, the consumption of oxygen at 362 K and the appearance of water at 366 K clearly indicate that oxidative dehydrogenation of ethoxy species to acetaldehyde occurred through the consumption of oxygen from the feed. On further temperature increases, significant oxygen consumption was accompanied by the formation of large amounts of water and CO_2 at 500 K, indicating total oxidation of the acetate and carbonate species by the oxygen in the feed. Obviously, the presence of oxygen in the carrier gas caused the sur-

face reaction of adsorbed ethoxy, acetate, and carbonate species to occur at much lower temperatures.

The TPSR profile of ethanol with the H_2O/O_2/He mixture showed similar features to those of the O_2/He carrier gas. Oxidative dehydrogenation of ethoxy species to acetaldehyde occurred at ~346 K. (Direct dehydrogenation of ethoxy species to acetaldehyde also may occur, as evidenced by the production of hydrogen at 370 K [23].) A fraction of the hydrogen produced was oxidized to water, as confirmed by the simultaneous consumption of oxygen at 370 K. The main consumption of oxygen at 504 K resulted in the formation of significant amounts of carbon dioxide and much smaller amounts of methane and carbon monoxide. This phenomenon indicated that the reactions of acetate and carbonate species with water and/or oxygen occurred in this temperature range. The acetate species might decompose into CH_4 and CO, and the carbonate species decomposed into CO_2. Again, the presence of oxygen in the carrier gas shifted the surface reactions of adsorbed ethanol to much lower temperatures.

3.3.3. TPD/TPSR comparison

Comparing the TPD and the TPSR profiles of adsorbed ethanol reveals some important features. Because ethoxy, acetate, and carbonate species were formed readily on adsorption of ethanol on the Ir/CeO_2 catalyst at room temperature, the surface reactions of these intermediates with oxygen species provided either by ceria or by the feed will determine the desorption features.

In the TPD case (i.e., absence of oxygen in the carrier gas), the ethoxy species underwent dehydrogenation to acetaldehyde at 552 K by interacting with the –OH groups on the CeO_2 surface. However, decompositions of acetate and carbonate species were the main reactions with increasing temperature. The addition of water to the carrier gas shifted the acetaldehyde desorption to 375 K and enhanced the acetate decomposition at ~623 K. In the presence of oxygen, the oxidative dehydrogenation of ethoxy species to acetaldehyde occurred at 350 K and the decomposition and oxidation of acetate and carbonate species occurred at ~500 K, a much lower temperature than when water and He was used as the carrier gas. This finding can be explained by the effective activation of gaseous oxygen on the Ir/CeO_2 catalyst. Thus, a permanent flux of activated oxygen will maintain the ceria surface in an oxidized state. As a result, ethoxy, acetate and carbonate species on the surface could be oxidized and/or decomposed readily at much lower temperatures. Meanwhile, the absence of acetone in the oxygen-containing atmosphere further confirms the rapid surface reaction/desorption of acetaldehyde.

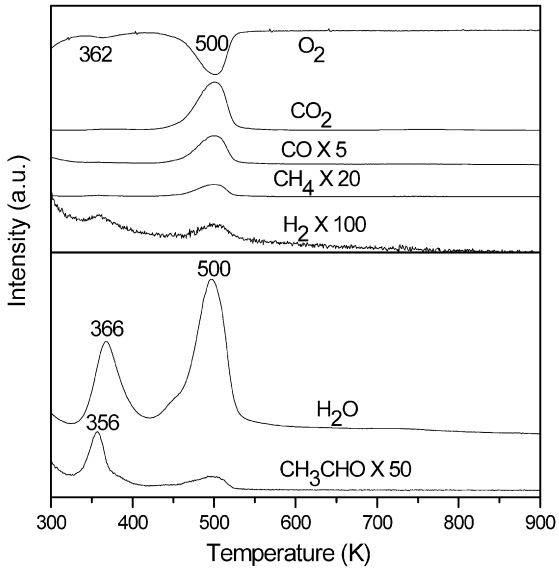

Fig. 6. Temperature-programmed surface reaction of adsorbed ethanol on the Ir/CeO_2 catalyst with a flow of 1.0% O_2/He stream.

Table 2 presents the carbon product yields estimated from the TPD/TPSR profiles of ethanol. In all cases, acetaldehyde and/or acetone, the minor products, were formed in the low-temperature region (350–550 K). The low acetaldehyde yield (only 15% [TPD] and 3 to 4% [TPSR] of the total carbon product yield) confirms that Ir was active for the carbon–carbon bond dissociation reaction. Here CO, CO_2, and CH_4 were the dominant products, desorbing at relatively higher temperatures. For TPD, these C1 products contributed to 81% of the total carbon product yield, and the high yields of carbon monoxide and methane suggested that decomposition of the acetate species was the main surface reaction. Under the TPSR conditions, however, CO, CO_2 and CH_4 contributed to more than 90% of the total carbon product yield with CO_2 as the major product, confirming the dominant presence of carbonate species.

3.4. Effect of temperature on SR, POX, and OSR of ethanol

Fig. 7 illustrates the product distribution from ethanol SR with a water/ethanol stoichiometric feed molar ratio of 3.0. The concentration of H_2 increased progressively with temperature. At temperatures below 673 K, acetaldehyde, acetone, and methane were formed. This confirms, as reported previously, that ethanol dehydrogenation to acetaldehyde was the primary reaction, and the acetaldehyde formed was further decomposed to methane and carbon monoxide or was converted to acetone through condensation. Once formed, CO likely reacted with water to produce H_2 and CO_2 through the water–gas shift (WGS) reaction. Ethanol, acetaldehyde, and acetone were entirely reformed into H_2, CO_2, CO, and CH_4 at 673 K. When the temperature was increased to 973 K, the concentration of H_2 approached 73% and the concentration of CH_4 decreased to 0.3% due to methane SR, as predicted by thermodynamics. The CO concentration increased monotonously up to 16%, and the CO_2 concentration to 10%, following the reversible WGS equilibrium,

$$C_2H_5OH \rightarrow CH_3CHO + H_2, \quad (4)$$

$$CH_3CHO \rightarrow CO + CH_4, \quad (5)$$

$$2CH_3CHO + H_2O \rightarrow CH_3COCH_3 + CO_2 + 2H_2. \quad (6)$$

Fig. 8 shows the results for POX of ethanol over the Ir/CeO_2 catalyst with an ethanol/O_2 molar ratio of 1:0.6. CO_2 was formed as the

Table 2
Product distributions for TPD and TPSR of ethanol

Product	Carbon yield (%)			
	He (TPD)	3.0% H_2O/He	1.0% O_2/He	3.0% H_2O/1.0% O_2/He
Carbon monoxide	45.1 (670 K)	5.2 (626 K)	6.9 (500 K)	8.9 (464, 536 K)
Carbon dioxide	9.8 (606 K)	68 (626 K)	83.8 (500 K)	81.8 (504 K)
Methane	26.5 (648 K)	17.2 (620 K)	6 (500 K)	5.4 (504 K)
Acetaldehyde	13.9 (552 K)	3.5 (375, 561 K)	3 (356, 493 K)	3.6 (346, 504 K)
Ethanol	0.6 (604 K)	2 (623 K)	0.3 (500 K)	0.4 (504 K)
Acetone	4.2 (552 K)	4.1 (375 K)	–	–

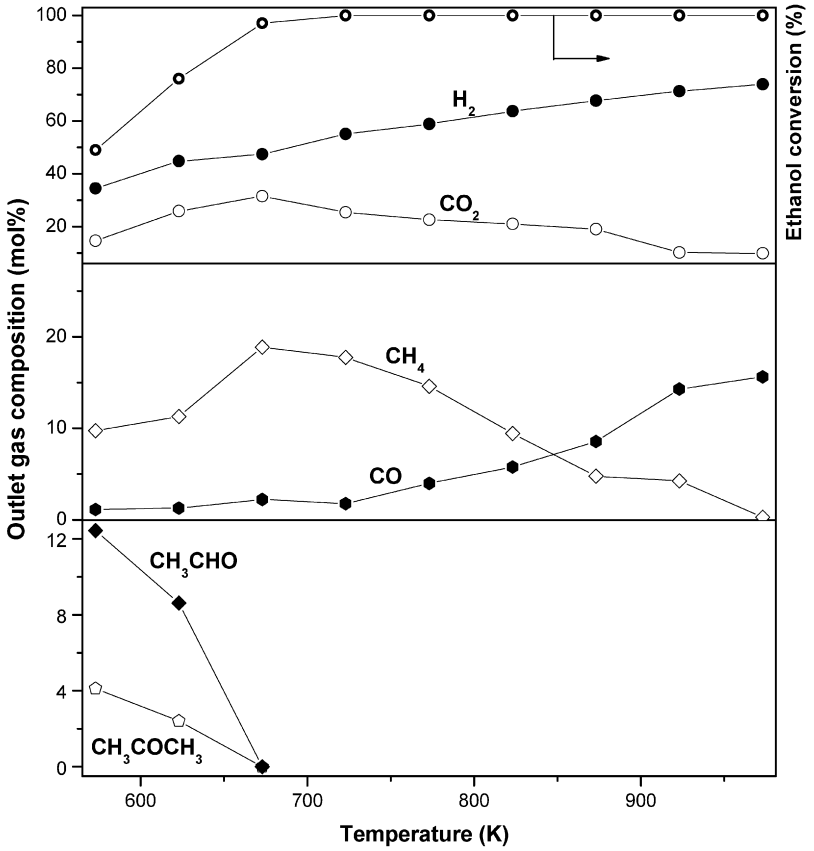

Fig. 7. Effect of reaction temperature on the product distribution for SR of ethanol over the Ir/CeO_2 catalyst. Reaction conditions: Ethanol/H_2O = 1:3.0, GHSV = 6000 ml/g_{cat}/h.

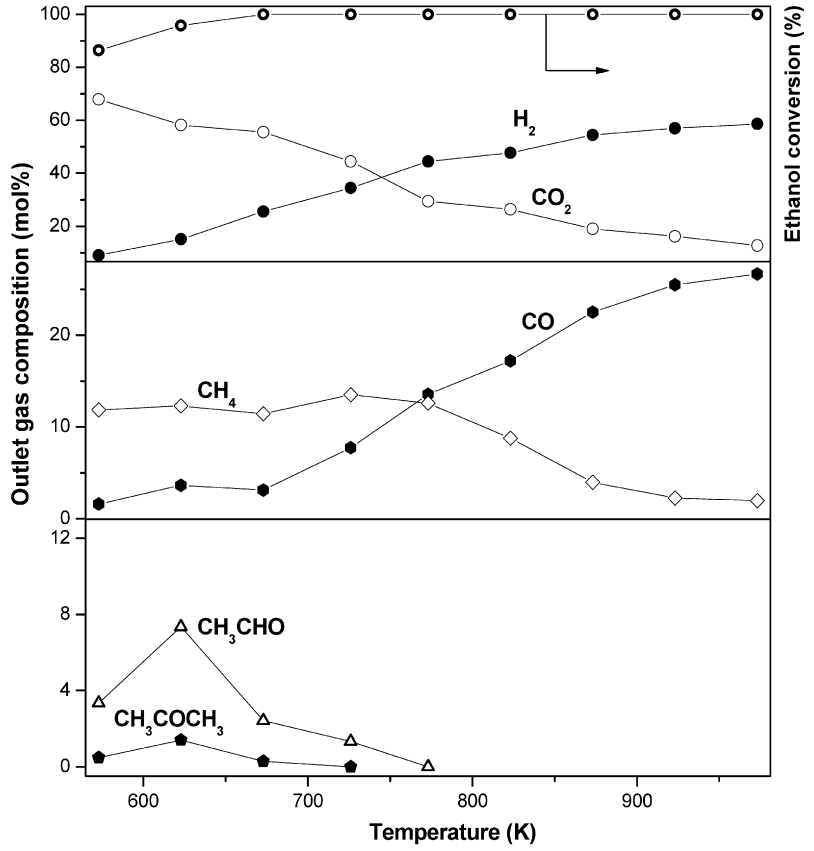

Fig. 8. Effect of reaction temperature on the product distribution for POX of ethanol over the Ir/CeO_2 catalyst. Reaction conditions: Ethanol/O_2 = 1:0.6, GHSV = 6000 ml/g_{cat}/h.

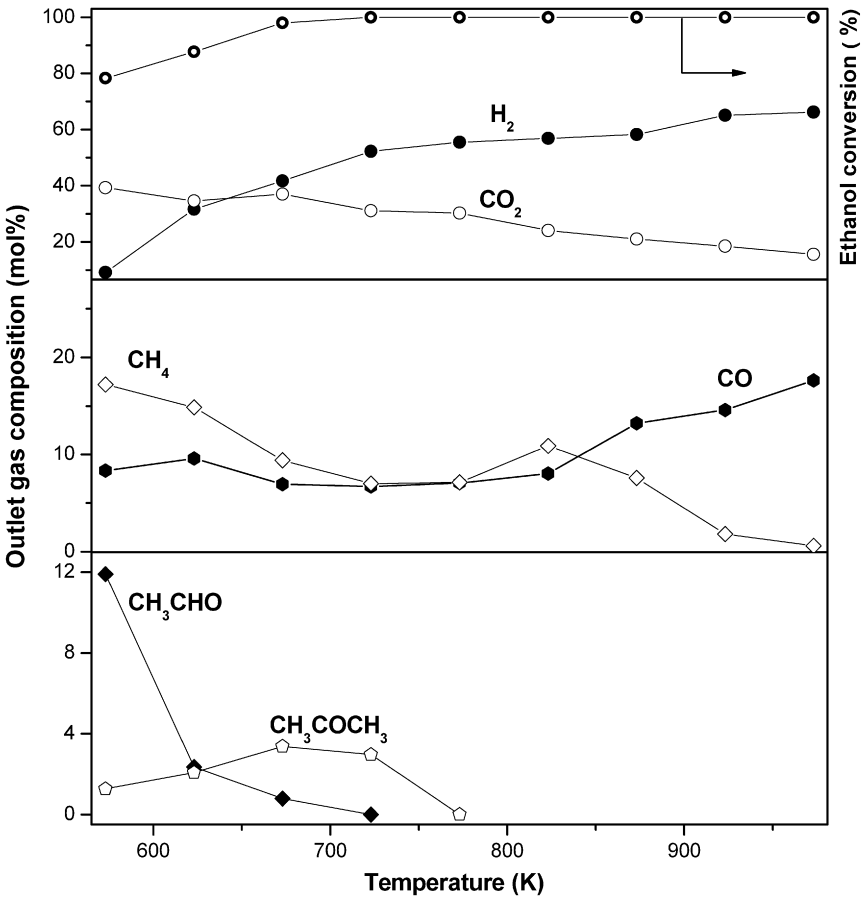

Fig. 9. Effect of reaction temperature on the product distribution for OSR of ethanol over the Ir/CeO_2 catalyst. Reaction conditions: $Ethanol/H_2O/O_2 = 1:1.8:0.6$, $GHSV = 6000\ ml/g_{cat}/h$.

dominant product at lower temperatures, indicating the enhanced oxidation of ethanol. Acetaldehyde also was produced by dehydrogenation of ethanol, and it disappeared completely at 773 K. The formation of acetone through condensation of acetaldehyde also was observed; it vanished at 723 K. The formation of CH_4 and CO indicates the decomposition of acetaldehyde. Complete conversion of ethanol, acetaldehyde, and acetone was achieved at 773 K. Above 773 K, the concentrations of methane and CO_2 decreased continuously due to methane reforming with carbon dioxide and/or water, and the relative concentrations of H_2, CO, and CO_2 were controlled by the reversible WGS equilibrium. At 973 K, the outlet gas comprised 56% H_2, 29% CO, 13% CO_2, and 1.5% CH_4.

Fig. 9 shows the product distribution of ethanol OSR with a stoichiometric composition of $ethanol/H_2O/O_2$ at a molar ratio of 1:1.8:0.6. In general, the OSR pattern appeared logically as a combination of SR and POX patterns. The concentration of hydrogen increased progressively with temperature, and the complete conversion of ethanol was achieved at 673 K. Significant amounts of CO_2 were formed at low temperatures due to the total oxidation of ethanol. The concentration of acetaldehyde decreased rapidly from 12% at 573 K to practically zero at 723 K. Meanwhile, trace amounts of acetone were produced through the condensation of acetaldehyde at 573 K, which disappeared at 773 K. The formation of methane through the decomposition of acetaldehyde was significant at 573 K, but the amount of CO was lower than that of methane, probably due to the WGS reaction. On a further temperature increase, the CO concentration dropped slightly whereas the CH_4 and CO_2 concentrations decreased more progressively. This clearly indicates that significant CH_4 reforming and the reverse WGS occurred. At 973 K, methane was almost completely reformed to hydrogen and carbon monoxide, and the outlet gas comprised 65% H_2, 18% CO, 16% CO_2, and 1% CH_4.

Table 3
Ethanol conversions and TOFs of SR, POX and OSR

Temp. (K)	Ethanol conversion[a] (%)			TOF[b] (s^{-1})		
	SR	OSR	POX	SR	OSR	POX
423	0.8	4.1	8.6	0.1	0.6	2.8
473	2.7	8.9	10.5	0.4	1.4	3.4

[a] $GHSV = 36{,}000\ ml/g_{cat}/h$.
[b] The average size of Ir particle was 2 nm, judged from the HRTEM images of the used catalysts.

Table 3 compares the turnover frequencies (TOFs) for the three reactions under differential conditions. As expected, the TOF of Ir followed the order POX > OSR > SR. The TOF of POX reaction was more than 10-fold greater than that of the SR reaction. This is consistent with the TPSR results demonstrating that the presence of oxygen greatly promoted the surface reaction of ethanol. It can be assumed that the lattice oxygen of ceria initially participated in the activation of ethanol and that the oxygen in the feed immediately supplemented the oxygen vacancies, which improved the reaction rate. In such a scheme, the reaction of ethanol occurs mainly at the CeO_2–Ir interface, where Ir is mainly responsible for breaking the C–C bond of ethanol and CeO_2 activates H_2O/O_2 and produces active oxygen to oxidize carbon species. Thus, the strong Ir–CeO_2 interaction favors these cooperative reaction steps and accelerates the conversion of ethanol.

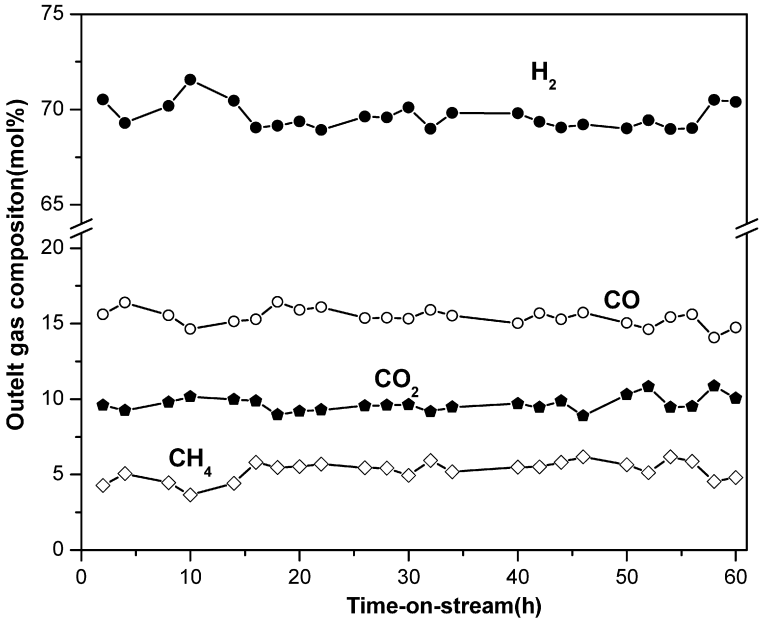

Fig. 10. Alteration of outlet gas composition for SR of ethanol over the Ir/CeO_2 catalyst. Reaction conditions: 923 K, ethanol/H_2O = 1:3, GHSV = 6000 ml/g_{cat}/h.

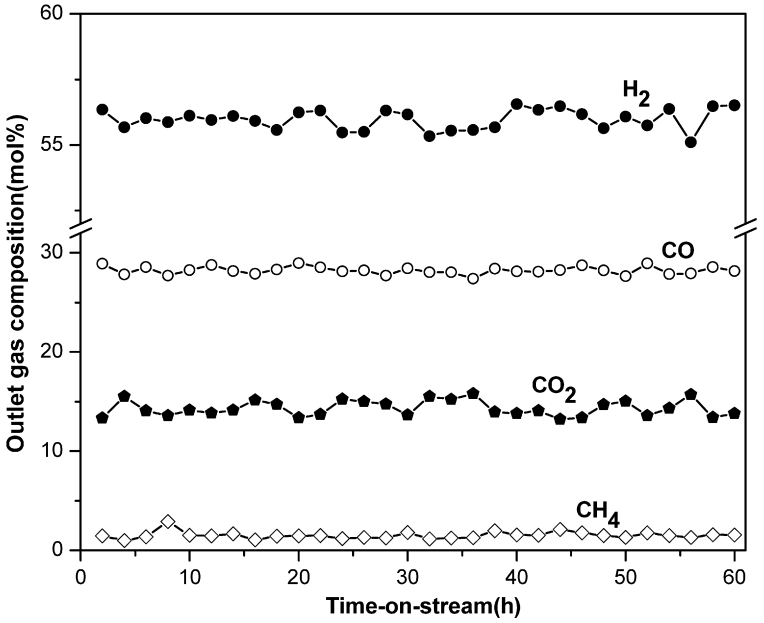

Fig. 11. Alteration of outlet gas composition for POX of ethanol over the Ir/CeO_2 catalyst. Reaction conditions: 923 K, ethanol/O_2 = 1:0.6, GHSV = 6000 ml/g_{cat}/h.

3.5. Stability test

The development of stable catalysts is one of the most important issues in the production of hydrogen from ethanol, particularly for stoichiometric feed compositions in which no excess water and/or oxygen is available to remove carbon deposits, which are detrimental to catalytic stability. Consequently, stability tests were conducted for the SR, POX, and OSR of ethanol over the Ir/CeO_2 catalyst at 823 and 923 K. Ethanol and the reaction intermediates (acetaldehyde and acetone) were entirely converted to CO, CO_2, and H_2, with only trace amounts of CH_4.

When operated at 823 K, the outlet gas compositions of the three reactions maintained very stable for 60 h on stream. The outlet stream for SR comprised 63% H_2, 18% CO_2, 9% CO, and 10% CH_4. The concentrations of H_2, CO_2, CO, and CH_4 in the outlet stream of OSR were 54, 26, 12 and 8%, respectively. For the case of POX, the outlet gas contained 45% H_2, 35% CO_2, 13% CO, and 7% CH_4; however, the concentration of methane in the outlet stream still relatively higher at this reaction temperature.

Figs. 10–12 show the concentrations of H_2, CO_2, CH_4 and CO in the outlet streams of the SR, POX, and OSR of ethanol up to 60 h on stream at 923 K. In all cases, there was no apparent deactivation, and the concentrations of H_2, CO, CO_2, and CH_4 followed the thermodynamics. The concentrations in the outlet stream of ethanol SR were about 70% H_2, 15% CO, 10% CO_2, and 5% CH_4. The outlet gas stream of ethanol POX contained 57% H_2, 26% CO, 15% CO_2, and 2% CH_4, and the concentrations in the outlet gas of ethanol OSR were 65% H_2, 18% CO_2, 15% CO, and 2% CH_4. Compared with the reaction results at 823 K, the concentration of methane decreased significantly due to methane SR, but the concentration

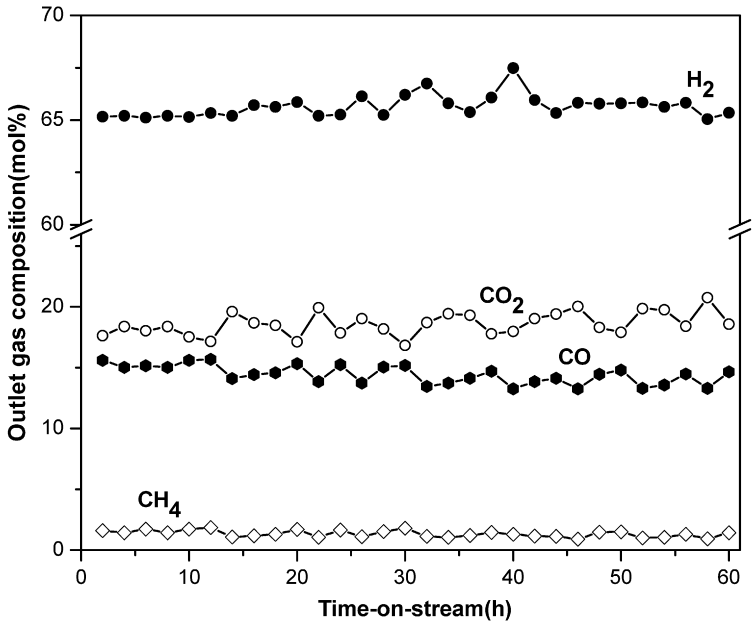

Fig. 12. Alteration of outlet gas composition for OSR of ethanol over the Ir/CeO_2 catalyst. Reaction conditions: 923 K, ethanol/H_2O/O_2 = 1:1.8:0.6, GHSV = 6000 ml/g_{cat}/h.

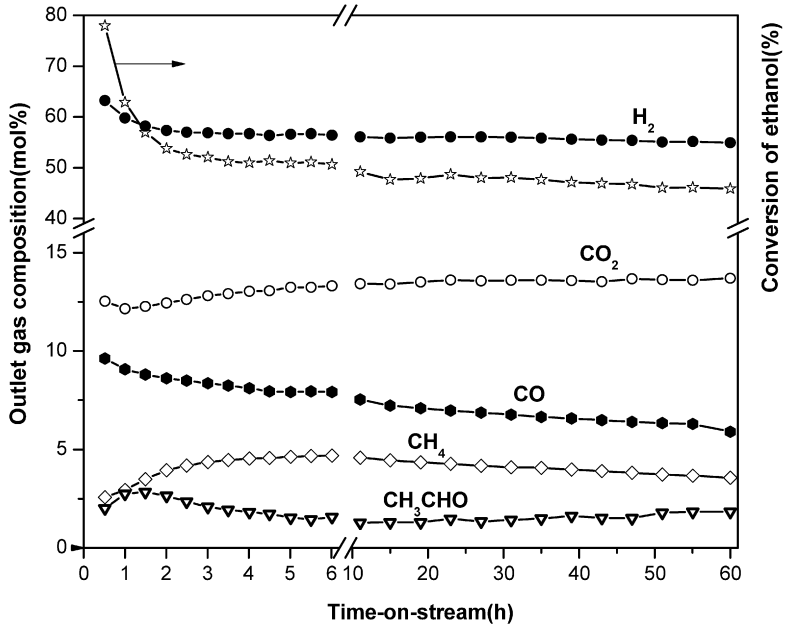

Fig. 13. Changes in the outlet gas composition for SR of ethanol over the Ir/CeO_2 catalyst. Reaction conditions: 923 K, ethanol/H_2O = 1:3, GHSV = 75,000 ml/g_{cat}/h.

of CO increased significantly due to the reverse WGS reaction. Apparently, the Ir/CeO_2 catalyst exhibited excellent stability for both SR and OSR of ethanol, even with stoichiometric feed compositions.

Fig. 13 illustrates the results of ethanol SR at 923 K under very high GHSV (75,000 ml/g_{cat}/h) ensuring partial conversion of ethanol and C_2 intermediates, which can be considered the most demanding condition in term of stability. The activity decreased significantly during the initial 3 h on stream and then became quite stable, with only marginal deactivation over the remaining testing period. There was little fluctuation in the product distribution, indicating high stability of the Ir/CeO_2 catalyst even under these severe conditions. In this high-GHSV operation in which the reactions occur far away from thermodynamic equilibrium, the production of acetaldehyde and methane remained 1.9 and 3.6%, respectively, confirming that acetaldehyde was a primary product. The initial deactivation might be due to reconstruction of the catalyst structure under the reaction conditions.

Fig. 14 shows the XRD patterns of the Ir/CeO_2 catalysts used for SR, POX, and OSR at 923 K. The absence of a diffraction peak of Ir indicates that no aggregation or sintering of Ir particles occurred during the tests. In contrast, the ceria crystallite size of ~6 nm in the fresh catalyst increased significantly, depending on the reaction atmosphere. For the SR and POX reactions, the ceria particle size increased to 22 and 27 nm, respectively, whereas for the OSR reaction it increased only slightly, to 14 nm. These changes in ceria size may explain, at least in part, the aforementioned rapid deactivation that occurred during the initial period under high GHSV. Nevertheless, it seems that the ceria particle size had no significant affect on the activity or stability of the Ir/CeO_2 catalyst. An association between the deactivation of ceria and the removal of

defects occurring at around 1033 K also has been suggested [40], but this process is not expected to occur under the present testing conditions.

Fig. 15 shows the HRTEM images of the used Ir/CeO_2 catalysts. Along with the significant increase in particle size, the morphology of the ceria particles also shifted from spherical in the as-prepared sample to polygonal crystallite cubes after the tests. The sample used for the OSR reaction appeared to be less agglomerated than those used for the SR and POX reactions, in agreement with the XRD measurements. The small ceria particles with high surface energy in the fresh catalyst likely tended to aggregate into large particles under the reaction conditions through a hydrothermal process [41]. The relatively small ceria particle size in the catalyst used for the OSR reaction might be due to the coexistence of H_2O and O_2 in the feed, which favored a slow sintering of ceria particles. The Ir particles with size of 2–3 nm remained highly dispersed on the surface of ceria for all conditions. This demonstrated that the strong Ir–CeO_2 interaction prevented sintering of the Ir particles during the course of the reaction.

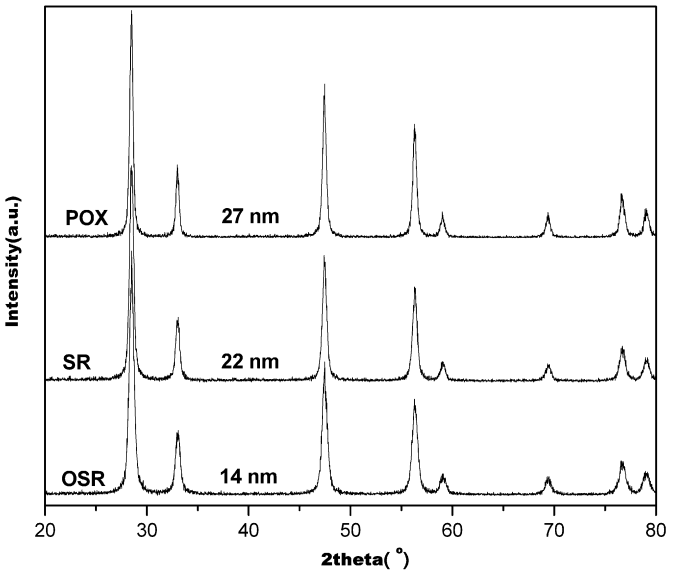

Fig. 14. XRD patterns of the Ir/CeO_2 catalysts used for POX, SR and OSR reactions at 923 K for 60 h on-stream.

No obvious carbonaceous deposits were observed in any of the cases. Fig. 16 shows the TPO profiles of the used catalysts for ethanol SR at 923 K. It is apparent that CO_2 was produced mainly at about 530 K by the oxidation of remaining reaction intermediates on the catalyst surface instead of coke, the removal of which often requires higher temperatures. The amount of carbon formed was almost negligible (3.3 mg C/g_{cat}). A similar phenomenon (carbon amount of 3.4 mg C/g_{cat}) was observed for the catalyst used only for 3 h on stream, demonstrating the presence of reaction intermediates on the catalyst surface and eliminating the possibility of coke deposition.

The significant deactivation reported for hydrogen production from ethanol reforming is usually attributed to carbon formation or sintering of metal particles, which is strongly influenced by the nature of the support and the reaction conditions (especially temperature and water/ethanol ratio) [9,39,42,43]. Information about the POX and OSR of ethanol is scarce, but carbon deposition also has been reported for POX over Pt/CeO_2 catalysts [31] and for OSR on Rh–Ni/CeO_2 catalysts [22]. Here the Ir/CeO_2 catalyst exhibited

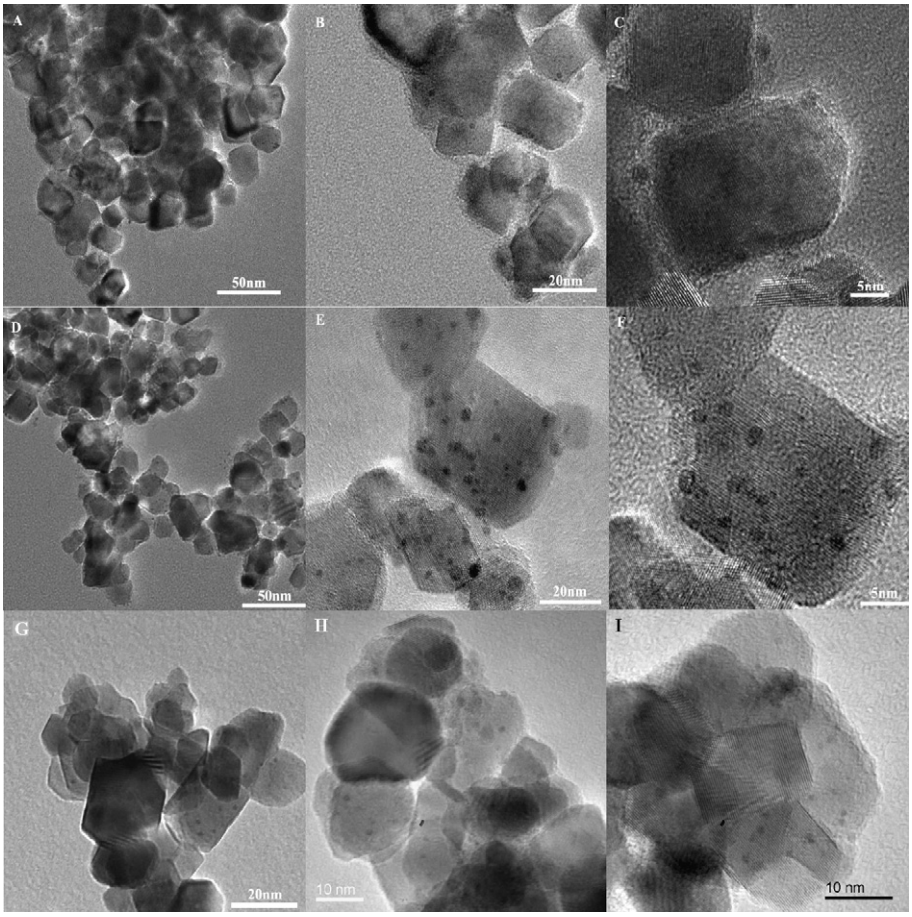

Fig. 15. HRTEM images of the Ir/CeO_2 catalysts used for POX (A–C), SR (D–F) and OSR (G–I) reactions at 923 K for 60 h on-stream.

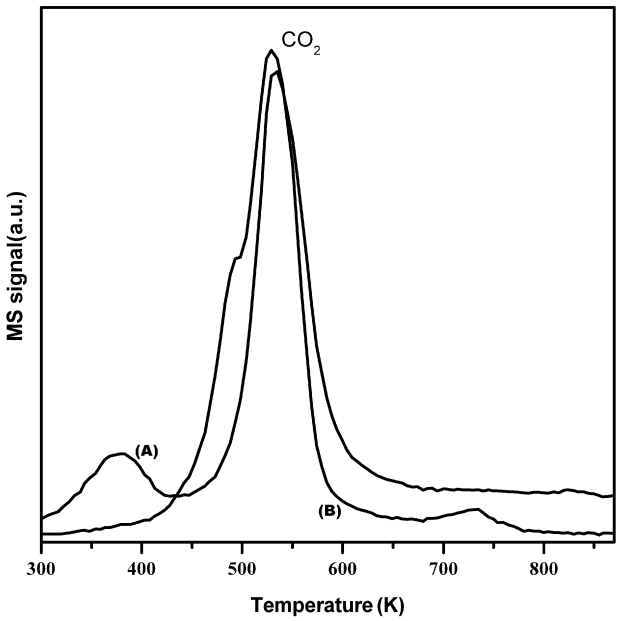

Fig. 16. Temperature-programmed oxidation of the used Ir/CeO_2 catalysts for ethanol SR at 923 K. (A) 3 h and (B) 60 h on-stream.

rather stable performance within 60 h on stream for both the SR and OSR of ethanol with stoichiometric feed compositions, obviously the most severe conditions for the catalytic tests. This can be explained by the effective removal of carbon from Ir particles, assisted by the promotional effect of ceria. As mentioned earlier, despite ceria sintering, the 2–3 nm Ir particles remained highly dispersed on the ceria surface, maintaining a sufficient Ir–ceria interfacial area where the reaction occurs, with a transfer of oxygen from ceria to Ir allowing continuous cleaning of carbonaceous entities. It seems that ceria particles in the range of 6–27 nm provide a sufficient Ir–CeO_2 interfacial perimeter, which favors facile activation of water and/or oxygen and easy transfer of oxygen species to Ir particles, promoting carbon removal.

4. Conclusion

The Ir/CeO_2 catalyst proved to be highly active and stable for the SR, POX, and OSR of ethanol. FTIR and TPSR measurements indicated that ethoxy species could be formed immediately on ethanol adsorption at room temperature, and that these species were then converted to acetate and carbonate species by interacting with ceria. With increasing temperature, the acetate species decomposed into methane and CO, whereas the carbonates converted to CO_2. Investigation of the reaction pathway revealed that dehydrogenation of ethanol to acetaldehyde was the primary reaction, and that acetaldehyde then decomposed to CH_4 and CO or converted to acetone at lower temperatures. Ethanol, acetaldehyde, and acetone were completely reformed to hydrogen and C1 products at 673–773 K. CH_4 and CO could be further converted into H_2 and CO_2 through methane reforming and the WGS reaction.

The Ir/CeO_2 catalyst demonstrated rather high stability for the SR and OSR of ethanol even with stoichiometric feed streams at 923 K for 60 h on stream, and there was no obvious deactivation with a constant effluent gas composition. Structural analysis of the used catalysts indicates that the 2–3 nm Ir particles remained highly dispersed on the enlarged ceria particles. But this sintering of ceria had no apparent influence on the activity or stability, because sufficient Ir–CeO_2 interface areas remained. Ceria likely prevented the highly dispersed Ir particles from sintering and effectively inhibited coke deposition through strong Ir–CeO_2 interactions.

Acknowledgment

Financial support was provided by the National Natural Science Foundation of China (Grant 20773119).

References

[1] D.K. Liguras, D.I. Kondarides, X.E. Verykios, Appl. Catal. B 43 (2003) 345.
[2] J.P. Breen, R. Burch, H.M. Coleman, Appl. Catal. B 39 (2002) 65.
[3] P.D. Vaidya, A.E. Rodrigues, Chem. Eng. J 117 (2006) 39.
[4] B. Zhang, X. Tang, Y. Li, W. Cai, Y. Xu, W. Shen, Catal. Commun. 7 (2006) 367.
[5] F. Aupretre, C. Descorme, D. Duprez, D. Casanave, D. Uzio, J. Catal. 233 (2005) 464.
[6] E.C. Wanat, K. Venkataraman, L.D. Schmidt, Appl. Catal. A 276 (2004) 155.
[7] C. Diagne, H. Idriss, A. Kiennemann, Catal. Commun. 3 (2002) 565.
[8] F. Auprêtre, C. Descorme, D. Duprez, Catal. Commun. 3 (2002) 263.
[9] A.N. Fatsikostas, X.E. Verykios, J. Catal. 225 (2004) 439.
[10] M.S. Batista, R.K.S. Santos, E.M. Assaf, J.M. Assaf, E.A. Ticianelli, J. Power Sources 134 (2004) 27.
[11] J. Llorca, N. Homs, J. Sales, P.R. Piscina, J. Catal. 209 (2002) 306.
[12] F. Frusteri, S. Freni, L. Spadaro, V. Chiodo, G. Bonura, S. Donato, S. Cavallaro, Catal. Commun. 5 (2004) 611.
[13] H.V. Fajardo, L.F.D. Probst, Appl. Catal. A 306 (2006) 134.
[14] H. Wang, J.L. Ye, Y. Liu, Y.D. Li, Y.N. Qin, Catal. Today 129 (2007) 305.
[15] J.R. Salge, G.A. Deluga, L.D. Schmidt, J. Catal. 235 (2005) 69.
[16] L.V. Mattos, F.B. Noronha, J. Catal. 235 (2005) 18.
[17] D.K. Liguras, K. Goundani, X.E. Verykios, J. Power Sources 130 (2004) 30.
[18] V. Fierro, V. Klouz, O. Akdim, C. Mirodatos, Catal. Today 75 (2002) 141.
[19] V. Fierro, O. Akdim, C. Mirodatos, Green Chem. 5 (2003) 20.
[20] V. Fierro, O. Akdim, H. Provendier, C. Mirodatos, J. Power Sources 145 (2005) 659.
[21] F. Frusteri, S. Freni, V. Chiodo, S. Donato, G. Bonura, S. Cavallaro, Int. J. Hydrog. Energy 31 (2006) 2193.
[22] J. Kugai, V. Subramani, C. Song, M.H. Engelhard, Y. Chin, J. Catal. 238 (2006) 430.
[23] W. Cai, B. Zhang, Y. Li, Y. Xu, W. Shen, Catal. Commun. 8 (2007) 1588.
[24] R.M. Navarro, M.C. Álvarez-Galván, M. Cruz Sánchez-Sánchez, F. Rosa, J.L.G. Fierro, Appl. Catal. 55 (2005) 229.
[25] S. Cavallaro, V. Chiodo, A. Vita, S. Freni, J. Power Sources 123 (2003) 10.
[26] G.A. Deluga, J.R. Salge, L.D. Schmidt, X.E. Verykios, Science 303 (2004) 993.
[27] B.D. Cullity, in: Elements of X-Ray Diffraction, second ed., Addison–Wesley, Menlo Park, CA, 1978, p. 102.
[28] A. Yee, S.J. Morrison, H. Idriss, J. Catal. 186 (1999) 279.
[29] A. Trovarelli, Catal. Rev. Sci. Eng. 38 (1996) 439.
[30] J. Mikulová, J. Barbier Jr, S. Rossignol, D. Mesnard, D. Duprez, C. Kappenstein, J. Catal. 251 (2007) 172.
[31] E.M. Sadovskaya, Y.A. Ivanova, L.G. Pinaeva, G. Grasso, T.G. Kuznetsova, A. van Veen, V.A. Sadykov, C. Mirodatos, J. Phys. Chem. A 111 (2007) 4498.
[32] L.V. Mattos, F.B. Noronha, J. Catal. 233 (2005) 453.
[33] P.Y. Sheng, A. Yee, G.A. Bowmaker, H. Idriss, J. Catal. 208 (2002) 393.
[34] A. Yee, S.J. Morrison, H. Idriss, J. Catal. 191 (2000) 30.
[35] G. Jacobs, R.A. Keogh, B.H. Davis, J. Catal. 245 (2007) 326.
[36] A. Yee, S.J. Morrison, H. Idriss, Catal. Today 63 (2000) 327.
[37] F. Giordano, A. Trovarelli, C. Leitenburg, M. Giona, J. Catal. 193 (2000) 273.
[38] S.M. Stagg-Williams, F.B. Noronha, G. Fendley, D.E. Resasco, J. Catal. 194 (2000) 240.
[39] L.F. de Mello, F.B. Noronha, M. Schmal, J. Catal. 220 (2003) 358.
[40] E. Mamontov, T. Egami, R. Brezny, M. Koranne, S. Tyagi, J. Phys. Chem. B 104 (2000) 11110.
[41] F. Zhou, X. Zhao, H. Xu, C. Yuan, J. Phys. Chem. C 111 (2007) 1651.
[42] M.A. Goula, S.K. Kontou, P.E. Tsiakaras, Appl. Catal. B 49 (2004) 135.
[43] A.N. Fatsikostas, D.I. Kondarides, X.E. Verykios, Catal. Today 75 (2002) 145.